

Mid-Infrared Source Multiplicity within Hot Molecular Cores traced by Methanol Masers

S. N. Longmore^{1,2}, M. G. Burton¹, V. Minier³ and A.J. Walsh¹

¹*School of Physics, University of New South Wales, Sydney, 2052, NSW, Australia*

²*Australia Telescope National Facility, CSIRO, Epping, 1710, Sydney, Australia*

³*Service d'Astrophysique, DAPNIA/DSM/CEA Saclay, 91191 Gif-sur-Yvette, France*

Accepted 2006 March 22. Received 2006 February 6

ABSTRACT

We present high resolution, mid-infrared images toward three hot molecular cores signposted by methanol maser emission; G173.49+2.42 (S231, S233IR), G188.95+0.89 (S252, AFGL-5180) and G192.60-0.05 (S255IR). Each of the cores was targeted with Michelle on Gemini North using 5 filters from 7.9 to 18.5 μm . We find each contains both large regions of extended emission and multiple, luminous point sources which, from their extremely red colours ($F_{18.5}/F_{7.9} \geq 3$), appear to be embedded young stellar objects. The closest angular separations of the point sources in the three regions are 0.79, 1.00 and 3.33'' corresponding to linear separations of 1,700, 1,800 and 6,000AU respectively. The methanol maser emission is found closest to the brightest MIR point source (within the assumed 1'' pointing accuracy). Mass and luminosity estimates for the sources range from 3–22 M_{\odot} and 50–40,000 L_{\odot} . Assuming the MIR sources are embedded objects and the observed gas mass provides the bulk of the reservoir from which the stars formed, it is difficult to generate the observed distributions for the most massive cluster members from the gas in the cores using a standard form of the IMF.

Key words: masers – stars:formation – techniques:high angular resolution – stars:early type – stars:mass function – infrared:stars.

1 INTRODUCTION

Massive stars play a fundamental role in driving the energy flow and material cycles that influence the physical and chemical evolution of galaxies. Despite receiving much attention, their formation process remains enigmatic. Observationally, the large distances to the nearest examples and the clustered mode of formation make it difficult to isolate individual protostars for study. It is still not certain, for instance, whether massive stars form via accretion (similar to low mass stars) or through mergers of intermediate mass stars.

Advances in instrumentation, have enabled (sub) arcsecond resolution imaging at wavelengths less affected by the large column densities of material that obscure the regions at shorter wavelengths. Recent observations exploiting these capabilities have uncovered the environment surrounding *individual* massive protostellar systems. From analysis of $\sim 2.3 \mu\text{m}$ CO bandhead emission, Bik & Thi (2004) have inferred Keplerian disks very closely surrounding (within a few AU) four massive young stellar objects, while interferometric, mm-continuum observations, find the mass-function of protostellar dust clumps lies close to a Salpeter value down to clump radii of 2000AU (Beuther & Schilke 2004). These high resolution observations point toward an accretion formation scenario for massive stars.

Further discrimination between the two competing models is possible by examining the properties, in particular the young stel-

lar populations, of hot molecular cores. The mid-infrared (MIR) window (7–25 μm) offers a powerful view of these regions. The large column densities of material process the stellar light to infrared wavelengths, and diffraction limited observations are readily obtained.

Recent observations indicate that class II methanol masers exclusively trace regions of massive star formation (Minier et al. 2003) and are generally either not associated or offset from UCH_{II} regions (Walsh et al. 1998). Minier et al. (2005) (hereafter M05) have carried out multi-wavelength (mm to MIR) observations toward five star forming complexes traced by methanol maser emission to determine their large scale properties. They found that maser sites with weak ($< 10\text{mJy}$) radio continuum flux are associated with massive ($> 50M_{\odot}$), luminous ($> 10^4 L_{\odot}$) and deeply embedded ($A_v > 40$ mag) cores characterising protoclusters of young massive (proto)stars in an earlier evolutionary stage than UCH_{II} regions. The spatial resolution of the observations ($> 8''$) was, however, too low to resolve the sources inside the clumps. Details of the regions from observations in the literature are described in M05. We have since observed three of the M05 regions at high spatial resolution to uncover the embedded sources inside the cores at MIR wavelengths.

2 OBSERVATIONS AND DATA REDUCTION

The data were obtained with Michelle¹ on the 8-m, Gemini North telescope in queue mode, on the 18th, 22nd and 30th of March 2003. Each pointing centre was imaged with four N band silicate filters (centred on 7.9, 8.8, 11.6 and 12.5 μm) and the Qa filter (centred on 18.5 μm) with 300 seconds on-source integration time. G173.49 and G188.95 were observed twice on separate nights and G192.60 observed once.

The N and Q band observations were scheduled separately due to the more stringent weather requirements at Q band. The standard Chop-Nod technique was used with a chop throw of 15'' and chop direction selected from MSX images of the region, to minimise off-field contamination. The spatial resolution calculated from standard star observations was $\sim 0.36''$ at 10 μm and $\sim 0.57''$ at 18.5 μm . The 32''x24'' field of view fully covered the dust emission observed by M05 in each region.

Particular care was taken to determine the telescope pointing position but absolute positions were determined by comparing the MIR data to sensitive, high resolution, cm continuum, VLA images of the 3 regions (Minier et al. in prep). Similar spatial distribution and morphology of the multiple components allowed good registration between the images. The astrometric uncertainty in the VLA images is $\sim 1''$.

Flux calibration was performed using standard stars within 0.3 airmass of the science targets. There was no overall trend in the calibration factor as a result of changes in airmass throughout the observations. The standard deviation in the flux of standards throughout the observations was found to be 7.4, 3.1, 4.4, 2.4 and 9% for the four N-band and 18.5 μm filters respectively. The statistical error in the photometry was dominated by fluctuations in the sky background. Upper flux limits were calculated from the standard deviation of the sky background for each filter and a 3σ upper detection limit is used in Table 1. Similarly, a 3σ error value is quoted for the fluxes in Table 1 (typical values for the N and Q band filters were 0.005 and 0.03 Jy respectively). The flux densities for the standard stars were taken from values derived on the Gemini South instrument, T-ReCS² which shares a common filter set with Michelle.

Regions confused with many bright sources were deconvolved using the Lucy-Richardson algorithm with 20 iterations. This was necessary to resolve source structure and extract individual source fluxes. The instrumental PSF was obtained for each filter using a bright, non-saturated standard star. The results were reliable and repeatable near the brighter sources when using different stars for the PSF and observations of the objects taken over different nights. As a further check, the standard stars were used to deconvolve other standards and reproduced point sources down to 1% of the peak value after 20 iterations, so only sources greater than 3% of the peak value were included in the final images. The resulting deconvolutions are shown in Fig 1.

3 DERIVING PHYSICAL PARAMETERS

A colour temperature was derived for each object, assuming the flux was greybody emission from dust at a single temperature and emissivity given by $1 - e^{-\tau_\lambda}$. τ_λ was calculated using A_v (from M05) and the Draine (1989) normalised silicate profile

($\tau_{12\mu\text{m}} = \tau_{18\mu\text{m}} = 0.022A_v$). The 12.5 to 18.5 μm flux ratios were used to derive the temperature as they are expected to contain the least PAH emission and are less affected by the broad-band silicate absorption features. In cases where either the 12.5 and 18.5 μm source flux was below the detection limit, only an upper and lower temperature limit respectively was derived. Luminosities were derived in the blackbody limit at the calculated source colour temperature. The values agreed to $< 1\%$ with those calculated by integrating the product of the Planck function and the emissivity function from 1-600 μm so provide a reasonable lower limit to the bolometric luminosity (De Buizer et al. 2005). Luminosities derived from colour temperatures agree well with those from radiative transfer model fits to the SED across the near and MIR (De Buizer, priv. comm.). A mass estimate for the sources was calculated by considering the range of plausible α values in a mass luminosity-relationship, $L \propto M^\alpha$, for a deeply-embedded, zero age main sequence star. For stars on the main sequence $< 20M_\odot$, $\alpha = 3.45$ (eg Allen (1975)), while for stars $> 20M_\odot$, $\alpha \sim 3$ (Zinnecker 2003). Additional luminosities due to accretion (accounting for up to half the total luminosity (Osorio et al. 1999)) may increase α up to ~ 4 . Over this range of α ($3 < \alpha < 4$), a factor of ten error in luminosity corresponds to only a factor of ~ 2 in the calculated mass. An intermediate value, $\alpha = 3.45$, was chosen to derive the mass estimate. Flux errors of 20% and a 20% distance uncertainty corresponds to a colour temperature error of 10% and luminosity error of 35%. However, the relative luminosity uncertainty for sources within a core drops to 20% as they lie at the same distance. Using the 3σ upper flux limits from the 12.5 and 18.5 μm images the lower mass detection limit is $\sim 1M_\odot$ for an object at a typical observed source temperature of 130K at 1.8 kpc. The source positions, fluxes and derived properties are shown in Table 1.

4 RESULTS AND DISCUSSION

Figure 1 shows the 18.5 and 7.9 μm images of the three regions. The insets show deconvolved 7.9 μm images toward bright, confused regions. All the sources toward each region are assumed to belong to the same protocluster due to their sharply rising MIR flux ($F_{18.5}/F_{7.9} \gtrsim 3$) and large optical depths ($A_v > 40$ mag). Although $F_{18.5} \sim F_{7.9}$ for G192.60:2 1, the spectral energy distribution peaks in the MIR so it must still be heavily embedded. Due to the low signal to noise of the detection G173.49:1 5 was not included in the following analysis.

Table 1 lists the positions, morphology, measured fluxes and derived properties of the detected MIR sources and Table 2 shows the large scale clump properties derived in M05. In all three clumps, the individual source radii derived from the black body assumption compare well to the observed radii. The variation in individual source radii and temperature compared to the M05 values in Table 2 is not unexpected due to the M05 assumption of a single powering source. With a factor of ~ 2 error in the M05 luminosity (see eg Purcell et al. (2006) for error analysis of two-component, greybody fitting) the total measured MIR luminosity (L_{mir}) for G188.95 and G192.60 accounts for the M05 total core luminosity (L_{tot}). The large discrepancy in G173.49, however, suggests there are undetected, luminous, cold source(s). Attributing the missing flux to a single source would correspond to a star of mass $\sim 20M_\odot$.

¹ The Michelle imager employs a Raytheon 320x240 pixel Si:As IBC array with a pixel scale of 0.099''.

² See <http://www.gemini.edu>

Source	R.A. (J2000)	Dec (J2000)	F _{7.9}	F _{8.8}	Flux (Jy) F _{11.6}	F _{12.5}	F _{18.5}	T _{col} K	L _{mir} 10 ² L _☉	M M _☉	R AU
G173.49:1 1 ^{p,m}	05 39 13.07	35 45 51.3	0.68±0.03	0.14±0.008	0.25±0.01	0.36±0.01	4.30±0.1	102	2.8	5	250
G173.49:1 2 ^{pe}	05 39 13.02	35 45 50.7	0.32±0.02	0.04±0.004	0.06±0.005	0.07±0.007	1.90±0.08	84	3.2	5	390
G173.49:1 3 ^e	05 39 12.93	35 45 51.2	0.07±0.01	0.02±0.004	0.09±0.007	0.05±0.006	1.52±0.07	81	2.9	5	400
G173.49:1 4 ^e	05 39 13.25	35 45 52.6	<0.006	<0.002	0.01±0.004	0.05±0.007	2.27±0.09	75	7.3	7	740
(G173.49:1 5 ^p	05 39 13.34	35 45 49.6	0.04±0.007	0.02±0.004	0.02±0.003	0.02±0.004	0.03±0.01	236	1.9	5	3)
G188.95:1 1 ^{p,m}	06 08 53.34	21 38 29.0	2.62±0.06	0.55±0.02	2.19±0.03	3.83±0.05	18.44±0.3	136	8.4	7	240
G188.95:1 2 ^p	06 08 53.38	21 38 28.3	1.00±0.04	0.59±0.02	0.69±0.02	0.21±0.01	3.02±0.1	97	3.6	6	310
G188.95:1 3 ^p	06 08 53.42	21 38 29.2	0.02±0.01	0.01±0.005	0.23±0.01	0.71±0.02	1.84±0.08	175	0.6	3	40
G188.95:1 4 ^p	06 08 53.49	21 38 30.5	0.32±0.02	0.03±0.004	0.21±0.009	0.49±0.02	1.34±0.06	171	0.5	3	40
G188.95:1 5 ^p	06 08 53.78	21 38 33.8	0.02±0.006	0.01±0.003	<0.004	0.01±0.002	<0.03	>51	-	-	-
G188.95:1 6 ^e	06 08 54.15	21 38 25.6	2.09±0.06	1.02±0.03	2.80±0.04	2.37±0.04	23.64±0.4	107	19	9	590
G192.60:2 1 ^{pe,m}	06 12 54.06	17 59 25.1	79.5±0.7	21.81±0.2	47.72±0.4	95.32±1.0	76.79±2.4	388	75	13	90
G192.60:2 2 ^p	06 12 53.90	17 59 25.7	6.62±0.1	3.9±0.05	7.88±0.08	11.09±0.1	16.27±0.5	240	72	13	80
G192.60:2 3 ^e	06 12 54.95	17 59 21.3	0.81±0.03	1.04±0.02	0.86±0.02	0.40±0.02	31.93±1.0	67	430	22	7060
G192.60:2 4 ^e	06 12 54.73	17 59 32.3	<0.005	<0.002	<0.003	<0.002	3.2±0.13	<44	-	-	-
G192.60:2 5 ^e	06 12 54.39	17 59 26.8	<0.005	<0.002	<0.003	<0.002	0.9±0.06	<51	-	-	-

Table 1. Positions, measured fluxes and derived properties of the detected mid-infrared objects in the three cores. T_{col} is the colour temperature of the source derived from the 12.5 and 18.5 μ m flux ratios. R and L_{mir} are the radius and luminosity of a greybody at temperature T_{col} . The table uses notation Gxxx.xx:a b for the sources, where Gxxx.xx is the formation region from M05, ‘a’ is the clump number from M05 and ‘b’ is the mid-infrared source number. The superscript p, pe and e in the first column, denote point sources, point sources with low level surrounding extended emission and extended sources respectively. The superscript m denotes the source closest in projection to the methanol maser. The radius in the final column is from the black body fit and is consistent with observations. The quoted errors and upper flux limits are 3σ values. Distances of 1.8, 2.2 and 2.6 kpc are used for G173.49, G188.95 and G192.60 respectively.

4.1 Nature of the MIR sources

MIR emission traces dust heated by nearby sources. Its morphology provides clues as to the nature of the source, in particular, whether the dust is heated externally or by an embedded source. Observationally, the sources fall into three morphological categories; (i) unresolved point sources, (ii) unresolved point sources with weak surrounding extended emission and (iii) extended emission, which we have designated in Table 1 as P, PE and E, respectively. The source morphology is consistent across the filter range (after deconvolution at longer wavelengths) but it is unclear whether G173.49:1 3 is actually a colder component of the extended emission surrounding G173.49:1 2 instead of a separate source.

With a spatial resolution ~ 400 AU we have made the assumption that the point-like sources (P and PE) are stellar in origin and the extended sources (E) are non-stellar (eg externally heated) with the exception that the most luminous source in the region is expected to be internally heated regardless of morphology. The internal heat sources are expected to be either very young stars or proto-stars. All non-stellar sources have been excluded from the analysis in §§4.2, 4.3 and 4.4.

4.2 Point source spatial distribution

As the large scale clump dust and gas morphology appears simple and centrally peaked (see M05), we make the reasonable assumption that the protocluster centres coincide with the central peak of dust emission. The spatial distribution of the point sources within the protocluster is similar between the clumps with close point sources toward the cluster centre. The methanol masers are found closest to the brightest MIR point source (within the assumed 1'' pointing error from image registration). These sources have temperatures sufficient to evaporate methanol ice from the dust grains into the gas phase (>90 K) as well as sufficient luminosity of IR

Clump	L_{tot} 10 ⁴ (L _☉)	L_{hot} 10 ² (L _☉)	L_{mir} 10 ² (L _☉)	M_{gas} 10 ² (M _☉)	T_{hot} (K)	R_{hot} (AU)	NH ₂ 10 ²² (cm ⁻²)
G173.49:1	4.9	3.7	18	1.2	122	200	16
G188.95:1	1.1	77	32	0.5	150	600	5
G192.60:2	5.1	390	577	3.2	225	600	22

Table 2. Properties of the three cores derived from M05 using a greybody approximation to fit the spectral energy distribution. L_{tot} is the total clump luminosity, L_{hot} , T_{hot} and R_{hot} give the luminosity, temperature and radius of the hot component derived from the greybody approximation. L_{mir} is the total luminosity of the sources in each core from Table 1. M_{gas} is the average gas mass derived from mm-continuum and molecular spectral line observations of the clumps. The NH₂ column densities are the values derived from mm-continuum observations in M05.

photons to pump the masing transition – conditions models suggest are required for such emission (Voronkov et al. 2005).

It is known that more massive stars favour cluster centres (e.g. de Grijs et al. (2002)), but it is unclear whether they form there or migrate in from outside. We have used the simple-harmonic model of ballistic motion developed by Walsh et al. (2004) to consider the motion of sources within the cores. Using the measured column density and radius from M05 (listed in Table 2), the time required for migration from the edge to the centre is $\sim 10^5$ years. This is comparable to the predicted HMC lifetime of 10^5 years (Kurtz et al. 2000) so we can not rule out the possibility of migration within the clumps. Any sources having migrated to the centre in this way would have acquired a velocity of ~ 2 kms⁻¹ with respect to the clump.

4.3 MIR source multiplicity

Massive stars in clusters are observed to have a high companion star fraction (Zinnecker 2003). In the M16 cluster, Duchêne et al. (2001) observed massive stars (earlier than B3) with visual companions separated by 1000-3000AU. If multiple systems are bound from birth, it is likely some of the sources we have observed will belong to multiple systems, even though the companions may lie below the detection limit. However, all three regions show two or more point sources at close angular separation (see insets of Figure 1) corresponding to linear separations of 1700 to 6000AU. We cannot determine whether these stars are physically bound or simply close due to projection effects but we can calculate the instrumental sensitivity required to confirm or deny the association. Assuming they are physically bound in a Keplerian orbit, the maximum proper motions (projection angle = 0°) of ~ 0.1 mas/year are too small to be detected on short temporal baselines. The maximum velocity difference (projection angle = 90°) ~ 2 kms $^{-1}$ is achievable by high spectral resolution observations of any line features.

4.4 Protocluster mass distribution

The mass distribution of stars is generally well described as a power law through the initial mass function (IMF). Given the mass of gas available to form stars, we may estimate the likelihood that a cluster will end up with the most massive stars that are observed in it. The fraction of gas that forms stars is given by the star formation efficiency (SFE) and is observationally found to be less than 50% in any cloud and to be $\leq 33\%$ for nearby embedded clusters (Lada & Lada 2003). For a cluster whose total stellar mass is 120 (50, 320) M_\odot (equivalent to the gas mass determined for the three cores), Weidner & Kroupa (2004) estimate that the mean maximum mass that a star may have in it is 10 (5, 20) M_\odot . This is comparable to the largest observed mass in two out of the three cases. However, we also observed several other stars in each cluster so can estimate the probability of generating stars of equal or greater mass than the remaining mass distribution. We did this by running Monte-Carlo simulations to populate 10^5 clusters using Salpeter (1955), Miller & Scalo (1979) and Scalo (1986) IMFs until the available gas mass was exhausted. We only considered clusters which contained a star of at least equal mass to the most massive observed. The simulations show that even using the Salpeter form of the IMF (most biased toward forming high-mass stars) and allowing 50% of the gas to form stars, it is difficult to generate the observed mass distributions (probabilities $\lesssim 10^{-2}$, 10^{-5} , 10^{-1} for the three cores respectively). By itself, this may not be significant for a single cluster. However, since the probability is low for all three sources studied, it is unlikely that the mass distribution of the most massive stars can be produced by sampling a standard form of the IMF from the reservoir of gas available for star formation. This conclusion would not hold if there was a substantial stellar mass already in the cluster that remains unseen, or if much of the original gas mass had already been dispersed from the core due to star formation. The former requires a SFE close to unity and given the relatively quiescent state of the cores, the latter seems unlikely.

5 CONCLUSIONS

A larger sample of young, massive protoclusters is required to draw general conclusions. However, in all three hot molecular cores traced by methanol maser emission we have found:

- Multiple, MIR sources which can be separated into three morphological types: unresolved point sources (P); unresolved point source with weak surrounding extended emission (PE) and extended sources (E).
- The point sources lie at close angular separations. Future high spatial and spectral resolution observations may be able to determine whether or not they are physically bound.
- The methanol masers are found closest to the brightest MIR point source (within the assumed $1''$ pointing accuracy).
- Cooler, extended sources dominate the luminosity.
- The time scale for a source at the core edge to migrate to the centre is comparable to the Hot Molecular Core lifetime, so it is not possible to rule out large protostellar motions within the core.
- From the derived gas mass of the core and mass estimates for the sources, Monte Carlo simulations show that it is difficult to generate the observed distributions for the most massive cluster members from the gas in the core using a standard form of the IMF. This conclusion would not hold, however, if most of the original gas has already formed stars, or has been dispersed such that the original core mass is much greater than now observed.

6 ACKNOWLEDGMENTS

S.L. would like to thank Alistair Glass, Scott Fisher, Tony Wong and Melvin Hoare for helpful discussion of the data and scientific input. We thank the anonymous referee for the thorough response and insightful comments. This work was made possible by funding from the Australian Research Council and UNSW. The Gemini Observatory is operated by the Association of Universities for Research in Astronomy, Inc., under a cooperative agreement with the NSF on behalf of the Gemini partnership: NSF (USA), PPARC (UK), NRC (Canada), CONICYT (Chile), ARC (Australia), CNPq (Brazil) and CONICET (Argentina).

REFERENCES

- Allen C. W., 1975, *Astrophysical Quantities*. Astrophysical Quantities (3rd ed.; Athlone: London)
- Beuther H., Schilke P., 2004, *Science*, 303, 1167
- Bik A., Thi W. F., 2004, *A&A*, 427, L13
- De Buizer J. M., Radomski J. T., Telesco C. M., Piña R. K., 2005, *ApJS*, 156, 179
- de Grijjs R., Gilmore G. F., Johnson R. A., Mackey A. D., 2002, *MNRAS*, 331, 245
- Draine B. T., 1989, *Interstellar extinction in the infrared*. *Infrared Spectroscopy in Astronomy*, Proceedings of the 22nd Eslab Symposium held in Salamanca, Spain, 7-9 December, 1988. Edited by B.H. Kaldeich. ESA SP-290. European Space Agency, 1989., p.93, pp 93+
- Duchêne G., Bouvier J., Eisloffel J., Simon T., 2001, in *ASP Conf. Ser. 243: From Darkness to Light: Origin and Evolution of Young Stellar Clusters* Statistical Properties of Visual Binaries as Tracers of the Formation and Early Evolution of Young Stellar Clusters. pp 399+
- Kurtz S., Cesaroni R., Churchwell E., Hofner P., Walmsley C. M., 2000, *Protostars and Planets IV*, pp 299+
- Lada C. J., Lada E. A., 2003, *ARAA*, 41, 57
- Miller G. E., Scalo J. M., 1979, *ApJS*, 41, 513
- Minier V., Burton M. G., Hill T., Pestalozzi M. R., Purcell C. R., Garay G., Walsh A. J., Longmore S., 2005, *A&A*, 429, 945

- Minier V., Ellingsen S. P., Norris R. P., Booth R. S., 2003, A&A, 403, 1095
- Osorio M., Lizano S., D'Alessio P., 1999, ApJ, 525, 808
- Purcell C. R., Balasubramanyam R., Burton M. G., Walsh A. J., Minier V., Hunt-Cunningham M. R., Kedziora-Chudczer L. L., Longmore S. N., + 27 authors 2006, MNRAS, 367, 553
- Salpeter E. E., 1955, ApJ, 121, 161
- Scalo J. M., 1986, Fundamentals of Cosmic Physics, 11, 1
- Voronkov M. A., Sobolev A. M., Ellingsen S. P., Ostrovskii A. B., 2005, MNRAS, 362, 995
- Walsh A. J., Burton M. G., Hyland A. R., Robinson G., 1998, MNRAS, 301, 640
- Walsh A. J., Myers P. C., Burton M. G., 2004, ApJ, 614, 194
- Weidner C., Kroupa P., 2004, MNRAS, 348, 187
- Zinnecker H., 2003, in IAU Symposium Formation of massive binaries. pp 80–

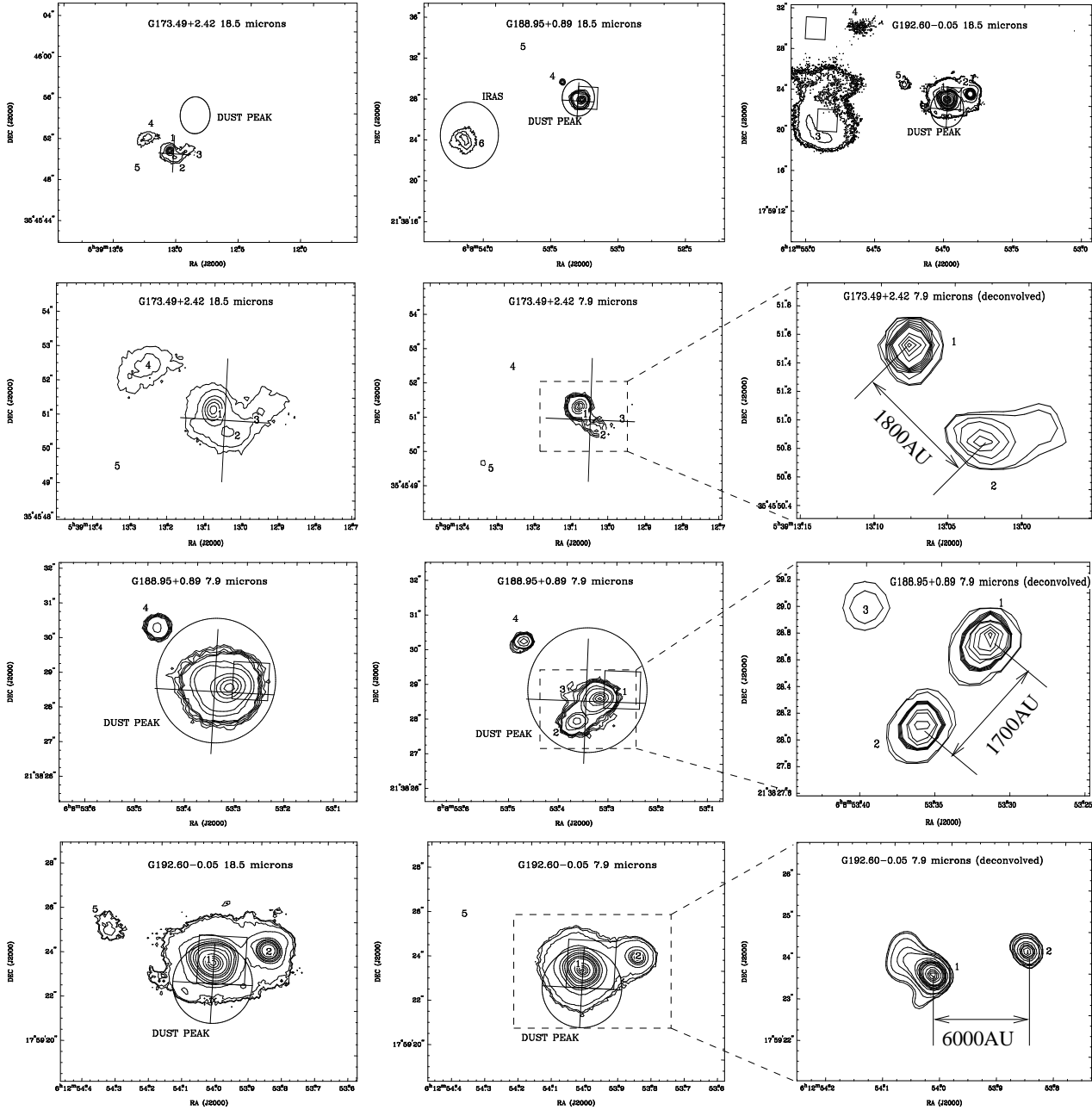


Figure 1. Images of the three regions. The top row displays the full field of view at 18.5 μm toward G173.49+2.42 Clump 1 (left), G188.95+0.89 Clump 1 (centre) and G192.60-0.05 Clump 2 (right). The centre of the mm dust peak emission from M05 is shown as an ellipse, methanol maser sites are shown as plus symbols and radio continuum sources as boxes. A further ellipse in the G188.95+0.89 images shows the position of the IRAS point source within the field but registration with a single MIR source is not possible due to the much larger IRAS beam size. The next three rows show close up images at 18.5 μm (left) and 7.9 μm (centre) of the bright point sources close to the dust peak and methanol maser emission (G173.49+2.42 (second row), G188.95+0.89 (third row) and G192.60-0.05 (bottom row)). The inset on the right shows the result when the boxed region in the 7.9 μm image is deconvolved with the instrument PSF. Scale bars in the deconvolved images give the linear separation of the sources assuming they lie at the same distance.